Numerical Simulations of a Severe Downslope Windstorm in Three Spatial Dimensions: Eddy-Kinetic-Energy Budget Analysis

By Terry L. Clark, National Center for Atmospheric Research, U.S.A.
Presented at the XVIII OSTIV Congress, Hobbs, N.M., U.S.A. (1983)

1.1 Abstract

Further analysis of the 3-D severe downslope windstorm simulation of Clark and Farley (1984) is presented. The present analysis compares the 3-D crossstream averaged velocity and temperature fields with those solutions previously obtained using 2-D models. The source/sink fields involved in the turbulent kinetic-energy budget are also presented.

The previous 2-D simulations produced very similar overall wave fields in a time-mean sense when compared to the present solutions. The 2-D simulations are, though, missing a significant transient character to the fields that results from a more realistic modelling of the turbulence in the 3-D solutions.

The turbulent kinetic-energy budget is shown to be dominated by the shear production terms. These terms act most strongly along the lower level of inflow into the super-adiabatic region (SAR) of the main forced gravity wave. The generated turbulence is advected throughout the SAR and finally results in eddies penetrating to the ground resulting in surface gustiness.

1. Introduction

As part of a physical application test of their numerical code, Clark and Farley (1984) presented a three spatial dimensional simulation of the 11 January (1972) Boulder Colorado windstorm. This windstorm was one of the few severe cases that has been observed by instrumented aircraft and is reported in Lilly and Zipser (1972) and Lilly (1978). The main simulation presented by Clark and Farley is that from which further analysis will be presented in this paper. Clark and Farley suggested that the convective breakdown of the super-adiabatic region (SAR) produced by the main forced gravity wave may be an important source of turbulence. It was also suggested in their paper that a competition existed between the surface wave forcing and the turbulent breakdown in the SAR resulting in a transient response to the surface gustiness. The period of this surface gustiness was approximately 10 to 20 min in this experiment and may represent the time scale of convective overturning in the SAR. Thus, it seems worthwhile to persue a better understanding of the dynamics that was occurring in the SAR through an analysis of the eddy (or turbulent) kinetic-energy budget. It is hoped that such an analysis will lead us to a better understanding of this important atmospheric phenomenon. The dynamics of severe windstorm is important not only to the general understanding of the dynamics of the atmosphere for purposes of physical parameterization and eventual improved predictions but also important to pilots so that they can better understand the nature of the phenomenon in which they sometimes fly.

There now exists a wealth of literature associated with the simulations of this particular windstorm. Klemp and Lilly (1978), Peltier and Clark (1979), Durran and Klemp (1983) and Hoinka (1985) all studied this event using two-dimensional numerical codes. These studies all produced similar strong surface wind speeds that exceeded 60 m/s which is in general agreement with the observations. The two-dimensional solutions did not, though, result in a gusty or transient character to the predictions of these winds but instead resulted in near steady final solutions. It is only with the introduction of the third spatial dimension that Clark and Farley (1984) were able to obtain a gusty character to the predicted surface winds. The frequency of the gustiness was, however, rather low in comparison to the observations. The reason may be attributed to a number of causes such as too coarse a spatial resolution, the use of the idealized bell-shaped topography or the use of two-dimensional far-upstream boundary conditions. The idealization of the natural event through numerical experiments does, though, greatly aid in developing our understanding of such events by allowing us to add one complication factor at a time and then assess the sensitivity of the solution to this particular factor.

2. Description of the Experiment

The model employed the three-dimensional equations of momentum

$$\rho \frac{dv_i}{dt} = -\frac{\partial p'}{\partial x_i} + \hat{k}\rho g\left(\frac{\theta'}{\bar{\theta}} - \frac{p'}{\bar{\gamma p}}\right) + \frac{\partial \tau_{ij}}{\partial x_j} \qquad (1)$$

and the dry air mass continuity equation

$$\frac{\partial(\rho v_i)}{\partial x_i} = 0 \qquad (2)$$

v is the i-th component of the three-dimensional wind where (x_1, x_2, x_3) represent the x (east-west), y (north-south) and z (vertical) directions, respectively. The main background flow is assumed to be in the x direction. p is the air density which is anelasticly approximated as a function of only z. p', p and 0', 0 are the perturbation and horizontally-uniform hydrostatically-balanced atmospheric pressures and potential temperatures, respectively. The stress tensor, τ_{ij}, represents the effects of subgrid scale mixing and from Smagorinsky (1963) and Lilly (1962) is taken as

$$\tau_{ij} = \rho K_M D_{ij} \qquad (3)$$

where the deformation tensor, D_{ij}, is defined as

$$D_{ij} = \frac{\partial v_i}{\partial x_j} + \frac{\partial v_j}{\partial x_i} - \frac{2}{3}\delta_{ij}\frac{\partial v_k}{\partial x_k} \qquad (4)$$

The eddy mixing coefficient, K_M, is approximated as

$$K_H = K_M = \begin{cases} \dfrac{(c\Delta)^2 |Def| (1 - Ri)^{1/2}}{\sqrt{2}} & \text{if } Ri < 0 \\ 0 & \text{otherwise} \end{cases} \qquad (5)$$

where Ri is a local Richardson number and where the total deformation Def is defined as

$$Def^2 = \frac{1}{2}\sum_i \sum_j D_{ij}^2 \qquad (6)$$

The first law of thermodynamics is taken as

$$\rho \frac{d\theta}{dt} = \frac{\partial}{\partial x_j}\left(\rho K_H \frac{\partial \theta}{\partial x_j}\right) \qquad (7)$$

where θ represents the total potential temperature, i.e. $\theta = \bar{\theta} + \theta'$.

There are many details not presented here which the interested reader can find in Clark and Farley (1984). Briefly stated, equations (1) to (7) are solved using finite-difference approximations. The equations are cast into a transformed coordinate system which allows for the treatment of the surface topography

$$h(x,y) = h_0/(1 + (x'/a)^2) \qquad (8)$$

which is assumed to have no variation in the y (or cross-stream) direction. h_0 and 'a' are taken as 2.044 and 10.0 km, respec-

tively. x_1 is the x distance from the domain centre of 120 km. Two models are used for the calculation in an interacting grid nesting sense. The outer model uses 122 by 12 by 42 grid points in the x, y and z directions with resolutions of 2.0, 1.0 and 0.8 km, respectively. The inner model uses 122 by 12 by 42 grids in the x, y and z directions with 1.0, 1.0 and 0.4 km, respectively. The time step varied between 8 and 5 seconds for both models. Cyclicity had been assumed in the cross-stream direction. Another assumption was the neglect of the Corriolis terms in (1).

3. Eddy-Kinetic-Energy Equation

One can form a turbulent kinetic energy equation by first defining all variables in terms of a y-direction average plus a deviation term. For example we let

$$v_i = \langle v_i \rangle + v_i' \qquad (9)$$
$$\theta' = \langle \theta' \rangle + \theta''$$

at any point where at positions x, z

$$\langle v_i \rangle = \frac{1}{L_y} \int_0^{L_y} v_i \, dy \qquad (10)$$

Variables, such as 0 and p which are already subdivided into perturbation and mean components, use a double prime to denote the eddy component. The eddy kinetic energy per unit volume is defined as

$$ke = \rho \, v_i' v_i'/2 \qquad (11)$$

and can be represented as a function of only x, z by considering <ke>. This definition of ke is a natural one for this particular experiment. In the case of purely two-dimensional flow both ke and <ke> become identically zero. Thus, the cross stream average <ke> represents the kinetic energy difference between the three and two dimensional y-direction averaged solutions.

Using (1), (2), (9) through (11), an eddy-kinetic-energy equation is derived as

$$\frac{\partial}{\partial t}\langle ke \rangle + \frac{\partial}{\partial x_1}\langle v_1' ke + v_1' p'' - \tau_{1j}' v_j' \rangle + \frac{\partial}{\partial x_3}\langle v_3' ke + v_3' p'' - \tau_{3j}' v_j' \rangle = + \langle p'' \frac{\partial v_i'}{\partial x_i} \rangle - \rho g \langle v_3' \rangle + \langle \frac{v_3' p''}{\bar{\theta}} \rangle + \ldots \qquad (12)$$

$$\ldots - \{\langle \rho v_1' v_i' \rangle \frac{\partial}{\partial x_1}\langle v_i \rangle + \langle \rho v_3' v_i' \rangle \frac{\partial}{\partial x_3}\langle v_i \rangle\} + \ldots$$

$$\ldots + g \langle \rho w' \frac{\theta''}{\bar{\theta}} \rangle - \langle \tau_{ij}' \frac{\partial v_i'}{\partial x_j} \rangle .$$

The first term on the left hand side of (12) represents the local-time derivative of the y-direction averaged turbulent kinetic energy and is a function of x, z, t. The remaining terms on the left hand side of (12) represent the effects of advection, pressure work and subgrid-scale diffusional transport. These three effects can be neglected when one is considering the domain-averaged budget of <ke> provided the domain is sufficiently large. In the present experiment the inner domain is only marginally large enough for such an approximation. The first term on the right-hand side of (12) represents a pressure-source term. When one uses the deep equations of Ogura and Phillips (1962) this term identically vanishes. Since the present model uses perturbation equations based upon an atmosphere of constant stability, this term is very small and negligible. The last three terms on the right-hand side of (12) represent the source/sink terms due to mean wind shear, buoyancy and eddy mixing (or dissipation), respectively. The effects of these three source/sink terms plus <ke> itself will be the main emphasis of the analysis.

4. Results from the Eddy Kinetic Energy Analysis

a. Mean y-direction-averaged 2-D solutions

Before showing the specific fields associated with the eddy-kinetic-energy equation, (12), the fields of <u>, <v>, <w> and <0> are shown in figs. 1 to 4. It is of considerable interest to researchers in this subject to understand how the introduction of the third spatial dimension affects the solutions. In this present three-dimensional simulation the vortext twisting and stretching terms are active, which fundamentally affects the dynamics of the modelled turbulence. It is of interest to know how this improvement in the modelling of the turbulence changes the results for the specific fluid dynamical phenomena of severe downslope windstorms from that which one would obtain using a 2-D model. In each of figs 1 to 4 are shown the times of 110, 125, 140 and 155 min. Fig. 1 shows <u> where we see the flow reversal aloft in the SAR. These solutions are quite similar to those obtained in the previously cited 2-D simulations for this particular event, (e.g.

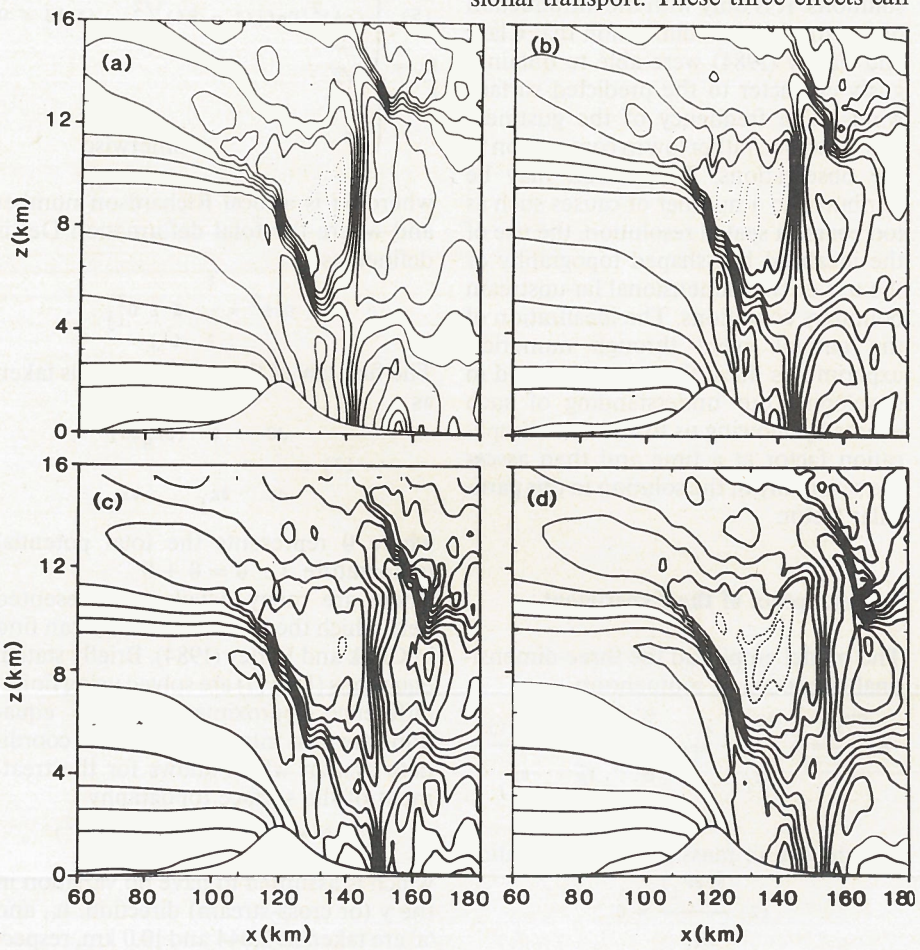

Fig. 1. Plots of cross stream averaged <u> for the inner model from experiment J11-FM3D from Clark and Farley (1984). Times shown are t = 110, 125, 140 and 155 min. Solid contours denote positive and dashed denote negative values. Zero contours are not shown. Contour interval is 8 m/s throughout. z = 0 in this and the following figures corresponds to about 1.6 km M.S.L.

fig 10 of Clark and Farley (1984)). One difference, due to the improved dynamics, is a transient character to the field of <u>. The magnitude of the minimum values of <u> are -21.9, -16.9, -10.6 and -22.3 m/s for 110, 125, 140 and 155 min, respectively. The maximum values of <u> are 66.4, 69.0, 75.4 and 79.1 for the same times. All of these values and the overall structure of <u> are quite similar to the 2-D solutions of the literature. The major difference between these and the earlier solutions is that now we have a distinct transient character in the SAR and downstream region due, I believe, to the more realistic modelling of the turbulence. Fig 2 shows the cross stream wind component <v> which reaches extrema of approximately ± 10 m/s. These fields are identically zero in the 2-D simulations and the domain average of <v> is similarly zero in this experiment. Note particularly how <v> originates in the SAR. This point is much clearer when one views plots obtained at slightly earlier times. Fig 3 shows up- and downdrafts. Particularly evident is the strong standing updraft in the lee of the mountain peak. The maximum values obtained in this updraft were 39.2, 39.0, 33.2 and 25.4 m/s. These are particularly strong values and probably represent small overestimates as discussed by Clark and Farley (1984). Finally fig 4 shows <0> for the four times. These solutions are again similar to the 2-D solutions but with a strong added transient character. One sees at the lee edge of the SAR almost vertical isolines of <0>. If one views the snapshots of 0 in the x-z plain in Clark and Farley then one sees distinct regions of overturning. The y-direction averaging has wiped out most of this effect. It is this tendency towards local overturning which makes the SAR so convectively unstable. It is also unstable because of the extreme values of shear produced along the SAR lower extremities.

b. <ke> and the source/sink fields.

Figs 5 to 8 show <ke>, buoyancy production, shear production and dissipation y-direction - averaged fields for the same four time levels as in figs 1 to 4. We see in fig 5 how <ke> first builds up in the SAR and maintains rather intense levels throughout this region for the remainder of the simulations. The most intense levels of <ke> occur along the lower extremities of the SAR which corresponds to the regions of most intense shear production. Some patches of <ke> can also be seen to occur outside the SAR where in plate (c) we see two regions of intense short lived <ke> occurring about 38 km downstream of the mountain peak. One region is aloft at about z = 10 km (near the tropopause) whereas the second region extends from the surface to about z = 6 km above the ground. The maximum level of <ke> occurrs in plate (c) and is approximately 226.0 kg (m · s^2).

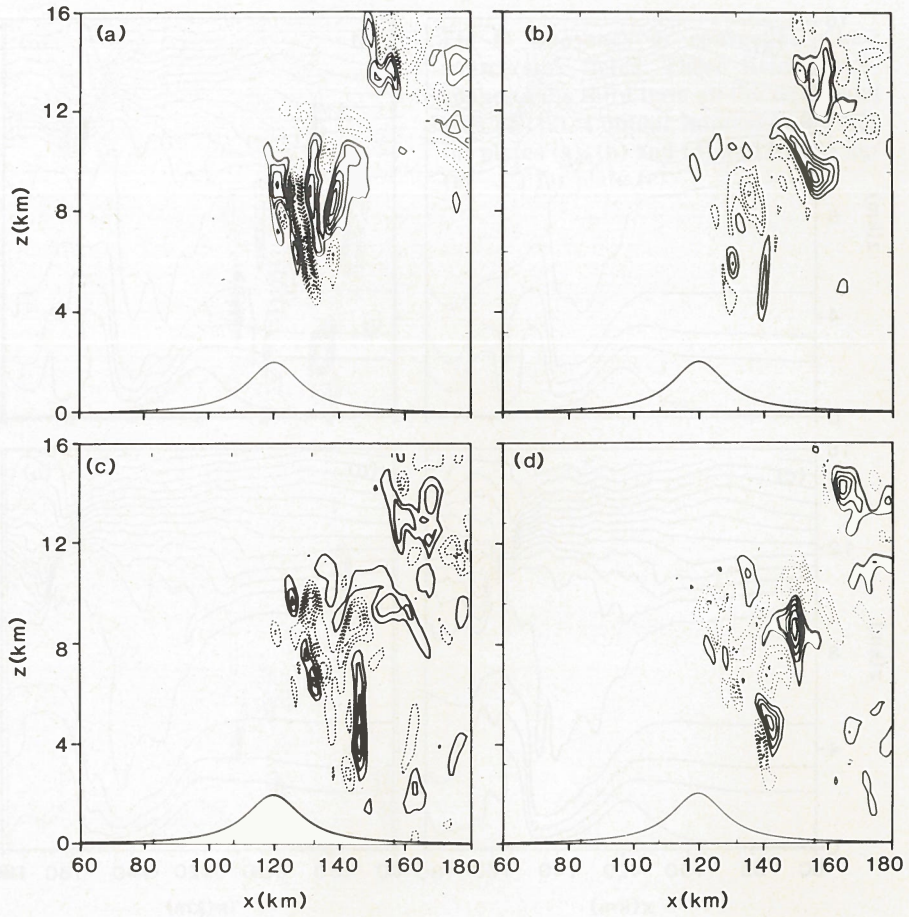

Fig. 2. Same as fig 1 except <v> is shown. Contour interval is (a) 1 m/s, (b) to (d) 2 m/s.

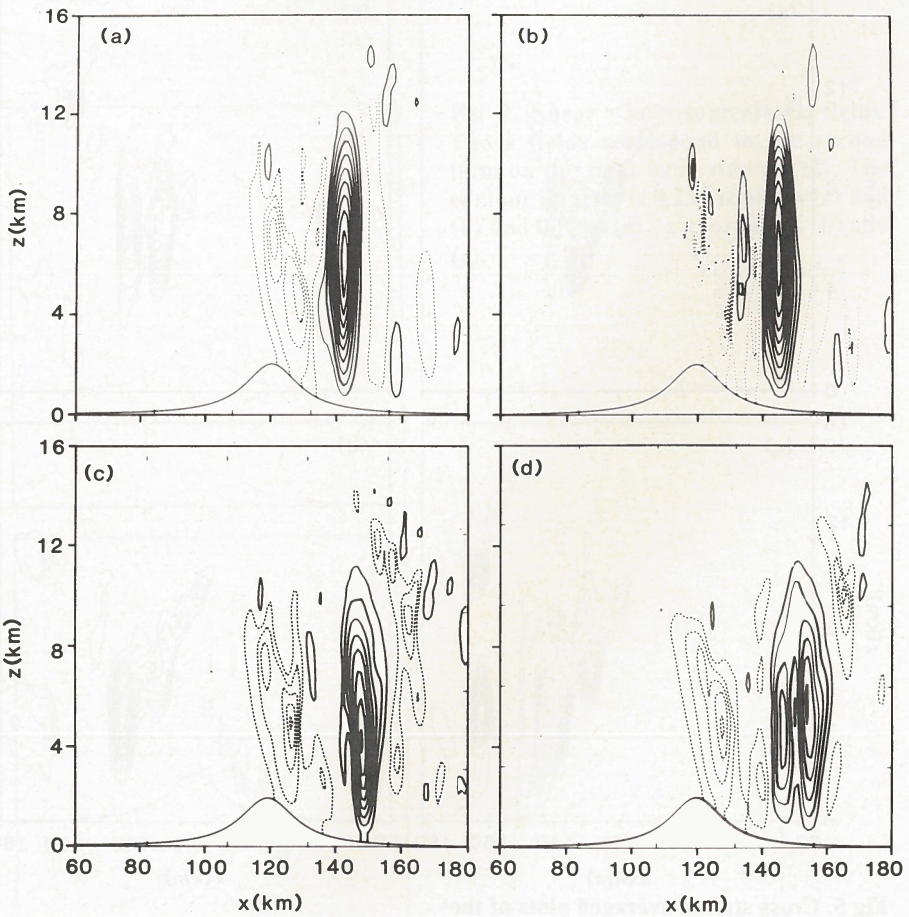

Fig 3. Same as fig 1 except <w> is shown. Contour interval is 4 m/s throughout.

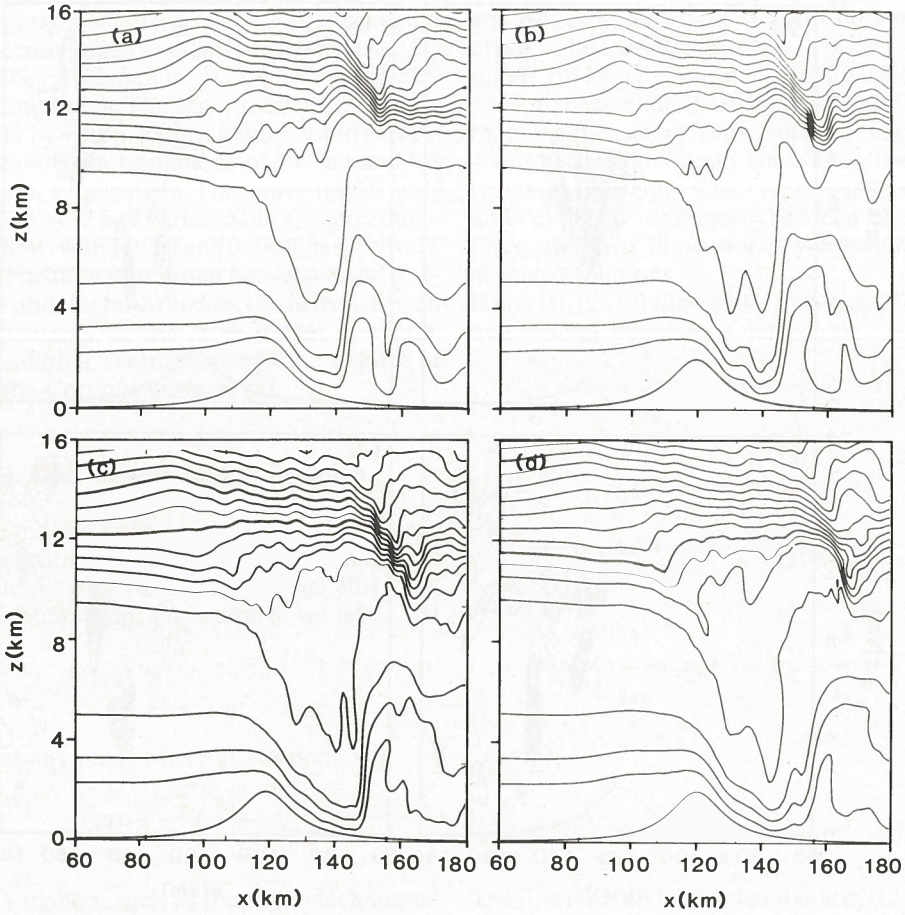

Fig 4. Same as fig 1 except <0> is shown. Contour interval is 8 Kelvins.

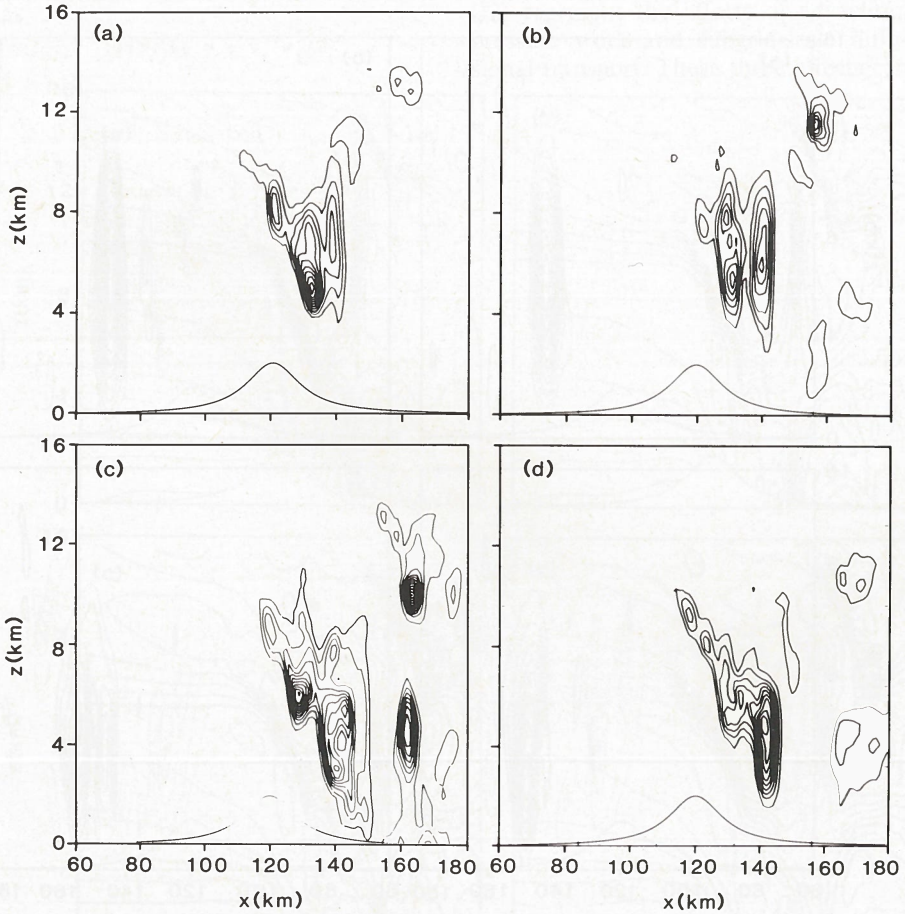

Fig 5. Cross stream averaged plots of the eddy kinetic energy density per unit volume <ke>. Same times as in figs 1-4. Contour interval is 16 kg/(m · s^2).

Fig 6 shows the convective production of turbulence. This source/sink term starts off producing most of <ke> in the developing SAR but after a short time (~ 5 min) the budget is dominated by the shear production terms. Note the intense regions of <ke> buoyant production that are located adjacent to the strong updrafts, i.e. compare figs 6(a) and 3(a) at t = 110 min. Although this buoyancy source/sink maintains its intensity throughout the simulation it appears to become rather patchy in structure once the turbulence is established.

Fig 7 shows field plots of the shear production of <ke>. This field is characterized by its most intense region, which corresponds to a source region, being strongly alligned with the streamlines flowing into the lower portions of the SAR that boarder the stable region below. The contour interval in fig 7 is almost 10 times that used for the convective source. The shear production is dominated by source regions whereas the buoyancy productionwas a mixture of source and sink regions.

Fig 8 shows the dissipation of<ke> which is due to the subgrid scale mixing terms. The dissipation regions, reasonably enough, correspond to the regions of existing <ke>. The typical intensity of dissipation is similar but smaller than the convective producton. Analytically and physically negative values of dissipation should not exist whereas is numerical models the truncation errors can be such as to allow some negative values. Negative values of dissipation did occur in this model but their values were negligible with respect to the overall budget. The obtained extrema for the dissipation were (.126,-.008), (.145,-.0006), (.1,-.01) and (.137,-.005) kg/(m · s^3) at t = 110, 125, 140 and 155 min, respectively. These values are significantly large when one considers that a value of 0.1, in the present units, corresponds to a value of greater than 1000 cm^2/s^3 in the more familar non-density-weighted dissipation rate. Even so the magnitudes of dissipation seem to be a little smaller than required to balance the strong shear production. This may be due to the fact that the analysis of the dissipation has not as yet included the effects of the model filters.

5. Conclusions

The cross-stream-averaged velocity fields and potential-temperature fields were presented and shown to be quite similar to those previously obtained using two-dimensional models. The main difference noted was the presence of a rather strong transient character in the 3-D solutions due to the improved modelling of the turbulence. Thus, while gustiness is not reproduced by the 2-D simulations, they do seem to agree quite well with the 3-D results on many of the important field characteristics.

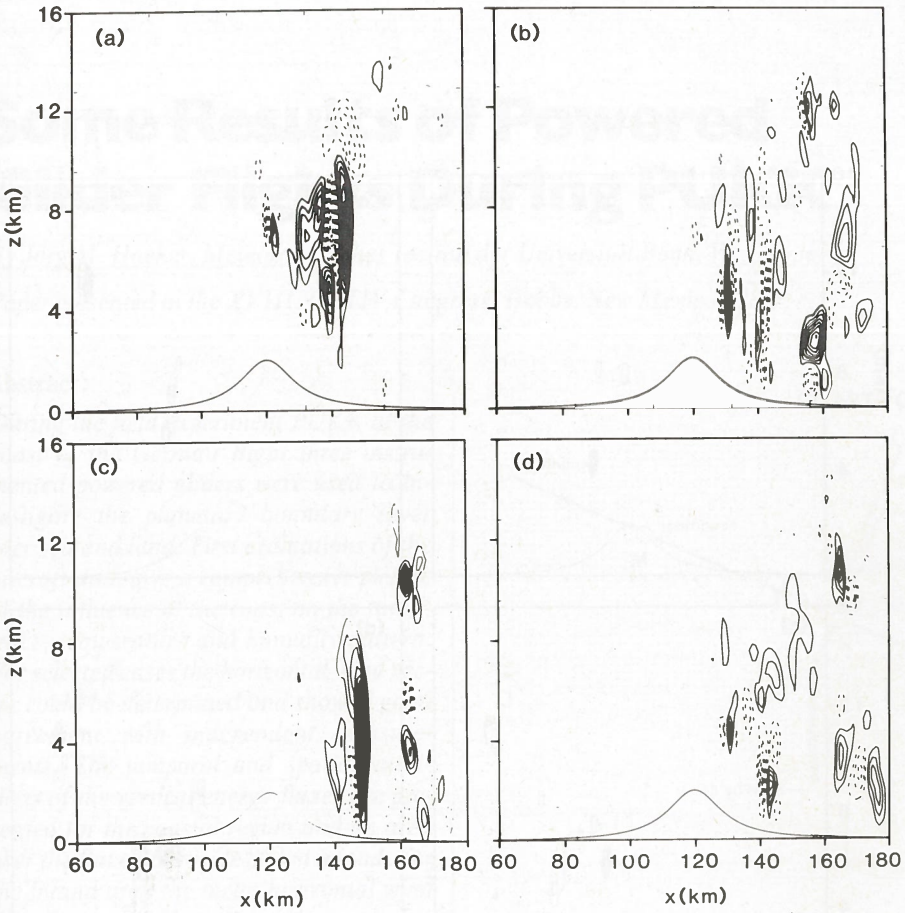

Fig 6. Buoyancy or convective <ke> source/sink fields. These fields correspond to the third term on the right hand side of (12). Contour interval is 0.03125 for plates (a), (b) and (d) and 0.0625 kg/(m · s^3) for plate (c).

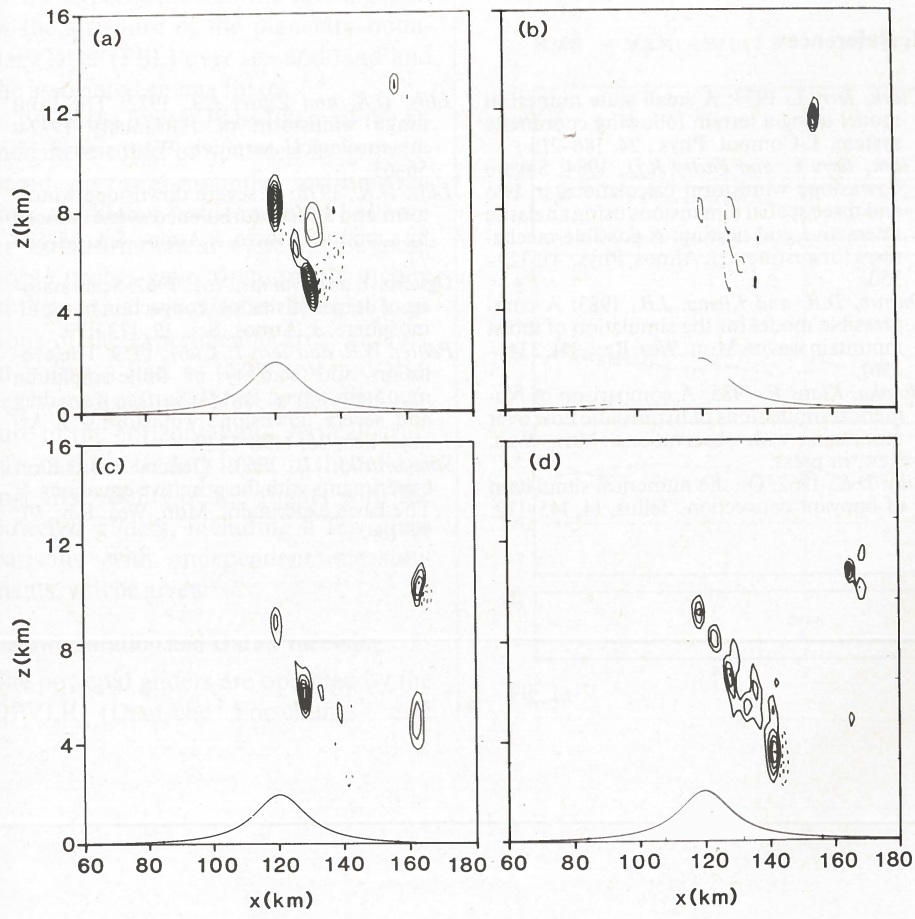

Fig 7. Shear <ke> source/sink fields. These fields correspond to the second term on the right hand side of (12). The contour interval is 0.25 for plates (a) and (d) and 0.5 kg/(m · s^3) for plates (b) and (c).

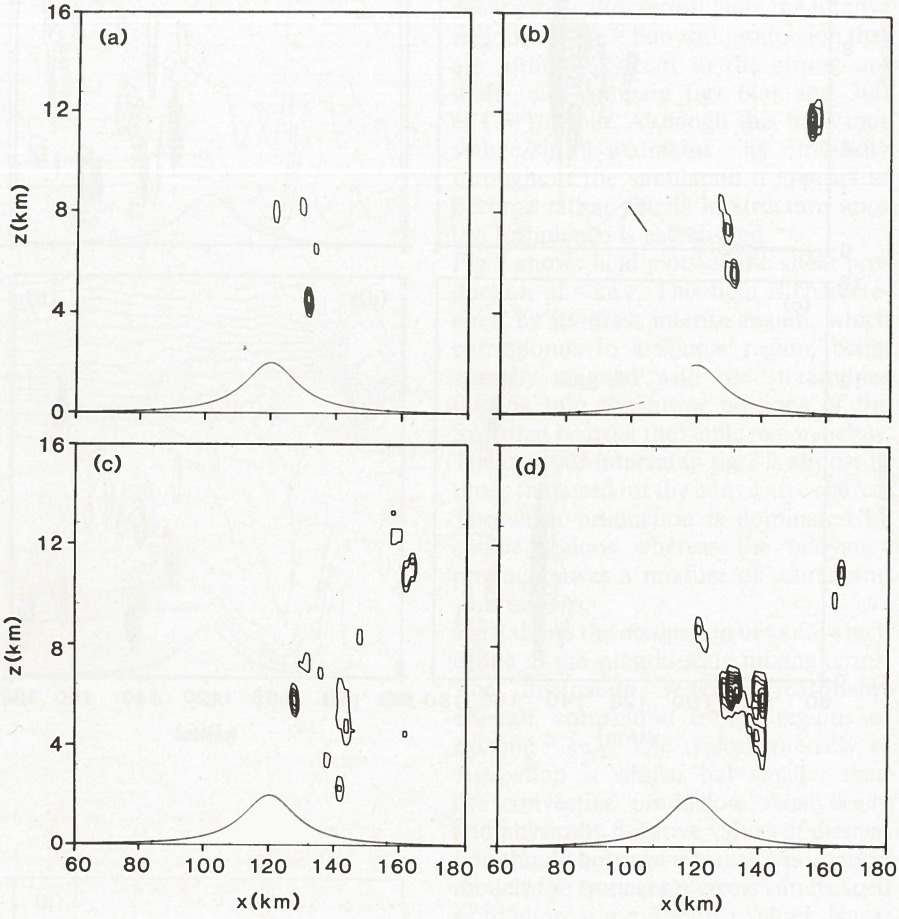

Fig 8. Dissipation <ke> sink fields. These fields correspond to the fourth term on the right hand side of (12). Contour interval is 0.0078125 kg/(m · s^3) throughout.

The production of the turbulence was shown to occur first in the super-adiabatic region (SAR) and then get advected throughout the SAR and finally get advected towards the surface. The buoyancy production was noted to initialize the turbulence production but only for a short period of time. Once turbulence had been produced the shear-production terms took over and dominated the eddy-kinetic-energy production budget.

The introduction of cross-directional variability in the topography, variable upstream forcing and higher spatial resolution would add further complexity to the simulation. Even with the present idealizations the simulated event is highly transient. The highly transient character of the SAR suggests that considerable care should be exercised in interpreting observations of such a situation obtained by local aircraft observations. The present simulation suggests that either ground-based or onboard remote wind sensing equipment is required to resolve such an event.

6. Acknowledgements

This paper was written while I was a guest scientist of the DFVLR in Oberpfaffenhofen, Germany. I sincerely appreciate the support that I received in the preparation of this manuscript.

7. References

Clark, Terry L. 1977: A small scale numerical model using a terrain following coordinate system. J. Comput. Phys., 24, 186–215

Clark, Terry L. and Farley R.D., 1984: Severe downslope windstorm calculations in two and three spatial dimensions using anelastic interactive grid nesting: A possible mechanism for gustiness. J. Atmos. Phys., 41, 329–350.

Durran, D.R. and Klemp, J.B., 1983: A compressible model for the simulation of moist mountain waves. Mon. Wea. Rev., 111, 2341–2361.

Hoinka, Klaus P., 1985: A comparison of Numerical simulations of hydrostatic flow over mountains with observations. Mon. Wea. Rev., in press.

Lilly, D.K., 1962: On the numerical simulatain of buoyant convection. Tellus, 14, 145–172.

Lilly, D.K. and Zipser E.J., 1972: The front range windstorm of 11 January 1972-a meteorological narrative. Weatherwise, 25, 56–63.

Lilly, D.K., 1978: A severe downslope windstorm and aircraft turbulence event induced by a mountain wave. J. Atmos. Sci., 35, 59–77.

Oguara, Y. and Phillips, N.A., 1962: Scale analysis of deep and shallow convection in the atmosphere. J. Atmos. Sci., 19, 173–179.

Peltier, W.R. and Terry L. Clark, 1979: The evolution and stability of finite-amplitude mountain waves. Part II: Surface wave drag and severe downslope windstorms. J. Atmos. Sci., 36, 1498–1529.

Smagorinsky, J., 1963: General circulation experiments with the primitive equations. I: The basic experiment. Mon. Wea. Rev., 91, 99–164.